The Impact of Defects on Tensile Properties of 3D Printed Parts Manufactured by Fused Filament Fabrication

Kazem Fayazbakhsh*, Mobina Movahedi, Jordan Kalman

Aerospace Engineering Department, Ryerson University, 350 Victoria Street, Toronto, ON, Canada M5B 2K3
**Corresponding author: kazem@ryerson.ca; Tel: (+1) 416-979-5000 ext. 6414; fax: (+1) 416-979-5056*

Abstract

Fused Filament Fabrication (FFF) is a popular 3D printing process that has gained interest from industry in a wide range of applications. This research work studies directional properties of FFF 3D printed PLA specimens per ASTM D638-14. Tensile strength, modulus, and failure strain of specimens along and transverse to the printing direction are evaluated. It is observed that FFF 3D printing introduces anisotropic behavior to the manufactured part, e.g. tensile strength of 57.7 and 30.8 MPa for loading along and perpendicular to the printing direction, respectively. FFF 3D printers, like other automated manufacturing techniques, introduce defects into fabricated parts considering their tolerances, e.g. in the form of missing materials leading to gaps. This study investigates the impact of gaps on tensile strength, modulus, and failure strain of 3D printed parts. Compared with the baseline, 20.5% reduction in tensile strength, 9.6% in modulus, and 11.5% in failure strain are observed due to missing extrudates (gaps) transverse to the loading direction. Experimental results from this study can be used as input data for Finite Element (FE) simulation and its verification.

Keywords:

Fused Filament Fabrication (FFF); 3D printing; tensile strength; tensile modulus; defects; gaps.

Materials Today Communications

https://doi.org/10.1016/j.mtcomm.2018.12.003

1. Introduction

Fused Filament Fabrication (FFF) is one of the most common additive manufacturing techniques to fabricate complex three-dimensional components to a near-net shape. The mechanical performance of FFF 3D printed parts depends on several manufacturing process and design parameters. Examples of manufacturing process parameters include machine tolerances, feedstock material, filament diameter, nozzle diameter, nozzle temperature, bed temperature, cooling rate (i.e. fan speed), and printing speed. On the other hand, examples of design parameters include build orientation, raster angle, layer thickness, and infill percentage.

Numerous studies investigated the impact of the aforementioned parameters on tensile strength and modulus of FFF 3D printed parts. Table 1 summarizes several studies and compares their findings regarding the impact of build orientation, raster angle, and layer thickness per ASTM D638 or ISO 527-2. It should be noted that results are extracted and presented in a way to make it possible to draw conclusions and make recommendations. First, the impact of build orientation is investigated [1-13], followed by raster angle [14-22], and layer thickness [23-27].

Table 1. The impact of design parameters on tensile strength and modulus of FFF 3D printed parts

Study	Filament Material	Build Orientation[1]	Raster Angle (degree)	Layer Thickness (mm)	Tensile strength (MPa)	Tensile modulus (GPa)
Ravindrababu, 2018 [1]	ABS[2] plus	XYZ XZY ZXY	0	0.1778	22.6 30.3 14.1	1.65 1.77 1.11
Chacón, 2017 [2]	PLA[3]	ZXY XZY XYZ	0	0.18	76.5 78.5 40.9	3.88 3.91 3.52
Zaldivar, 2017 [3]	ULTEM 9085™	XYZ XZY ZXY	45	3.2	46.83 71.03 38.48	2.01 2.48 2.03
Uddin, 2017 [4]	ABS	XYZ XZY ZXY	0	0.09	26.4 37.9 8.68	1.08 1.54 1.10
Smith, 2013 [5]	PC[4]	XYZ XZY ZXY	[-45/+45]	0.254	35.70 29.60 20.60	1.58 1.18 1.37
Abouziad, 2018 [6]	Copolyester	XYZ	45/-45 60/-30 75/-15 0/90	0.2	42.5 41.0 40.3 28.6	N/A[5]
Byberg, 2018 [7]	ULTEM 9085™	XYZ XZY ZXY	45/-45	0.254	70.6 75.8 31.3	N/A
Turk, 2017 [8]	ABS plus-P430	XZY ZXY	N/A	0.254	32.7 14.8	2.18 2.06
Discher, 2016 [9]	ULTEM 9085™	XYZ XZY ZXY	0	0.254	59.4 71.5 44.5	N/A
Love, 2014 [10]	ABS	XYZ ZXY	N/A	0.254	29.3 7.61	1.69 1.31

Bellini, 2003 [11]	ABS	XYZ XZY ZXY	[0/90/45/-45]	N/A	11.70 16.0 7.61	1.07 1.65 1.39
Safka, 2016 [12]	N/A	XYZ XZY	N/A	0.178	50.0 53.9	1.29 1.28
Zelený, 2014 [13]	ABS	XYZ XZY	N/A	0.25	20.82 22.16	N/A
Ziemian, 2015 [14]	ABS	XYZ	0 45 90 +45/-45	0.1778	25.15 10.11 9.16 16.90	1.49 1.04 1.04 1.28
Carneiro, 2015 [15]	PP[6]	XYZ	0 45 90 [0/90] [45/-45]	0.2	36.0 32.0 33.5 32.5 28.0	1.35 1.10 1.20 1.25 1.10
Hill, 2014 [16]	PC	XYZ	0 15 30 45 60 75 90	0.27	59.8 44.7 38.9 24.1 24.3 18.0 19.0	2.08 1.96 1.74 1.36 1.46 1.35 1.42
Dawoud, 2016 [17]	ABS	XYZ	[0/90] [30/-60] [45/-45] [75/-15]	0.5	33.1 33.2 34.5 33.6	N/A
Gajdoš, 2016 [18]	PC	ZXY	[0/0] [45/90]	0.127	23.08 35.25	N/A
Mahajan, 2015 [19]	Epoxy-CF[7]	XYZ	0 90	N/A	66.3 46.0	4.05 2.84
Chockalingam, 2016 [20]	ABS	XZY	0 30 60	0.4564	31.5 30.70 30.26	N/A
Lanzotti, 2015 [21]	PLA	XYZ	0 45 90	0.15	53.59 48.37 43.39	N/A
Ahn, 2002 [22]	ABS P400	XYZ	$[0]_{12}$ $[45/-45]_6$ $[0/90]_6$ $[90]_{12}$	0.5	19.7 11.8 12.2 2.77	N/A
Alafaghani, 2018 [23]	PLA	XYZ	+45/-45	0.2 0.3 0.4	59.0 61.7 48.8	3.13 3.82 27.1
Ning, 2016 [24]	ABS-5% CF	XYZ	[0/90]	0.15 0.2 0.25 0.3	34.5 33.3 31.9 22.8	1.11 0.877 0.844 0.696

				0.35	18.3	0.597
Garg, 2017 [25]	ABS	XZY	0/90	0.178 0.254 0.33	31.1 23 26.6	N/A
Vidakis, 2016 [26]	ABS	XYZ	0	0.25 0.33	18.1 16.2	N/A
Salem, 2015 [27]	ABS	N/A	N/A	0.1 0.2 0.3 0.4	34.5 30.0 28.7 27.6	1.80 1.71 1.61 1.61

1. Build orientation is defined per ISO/ASTM 52921:2013(E) [28]
2. Acrylonitrile Butadiene Styrene (ABS); 3. PolyLactic Acid (PLA); 4. PolyCarbonate (PC); 5. Not Available (N/A); 6. Polypropylene (PP); 7. Carbon Fiber (CF)

It can be concluded that specimens printed along XZY direction (on-edge) have the highest tensile strength and modulus, followed by XYZ (flat) and ZXY (up-right) [1-4, 5-6, 8-13]. The only exception is the work presented by Smith et al. [5], where they reported the highest tensile strength and modulus values for XYZ orientation. Considering raster angle, 0° orientation (along the loading direction) ensures the highest tensile strength and modulus, while 90° orientation (transverse to the loading direction) results in the lowest values [14, 16, 19-22]. An increase in the layer thickness causes a reduction in tensile strength and modulus [23, 26-27], while Garg and Bhattacharya [25] reported first a decrease and then an increase in the mechanical performance.

As it can be seen in Table 1, a systematic approach towards mechanical characterization of FFF 3D printed materials has not been followed. Researchers used excessive raster angle values and arbitrary layups that increased required number of testing (e.g., Hill and Haghi [16]) or limited findings to a specific layup (e.g., Dawoud et al. [17]). In addition, 3D printers like other automated manufacturing techniques create defects (gaps, overlaps, offset, etc.) into the final parts considering their tolerances. A careful review of the studies summarized in Table 1 or the work conducted by Popescu et al. [29] allows us to conclude that the impact of defects on the mechanical performance of 3D printed parts has not yet been investigated.

In this paper, first, tensile testing of 3D printed PLA specimens per ASTM D638 is performed to find material properties along and transverse to the extrudates. These values can then be used as input in Finite Element (FE) simulation software to model and optimize different layups per given loadings and boundary conditions. Tensile testing on a quasi-isotropic stacking sequence, here $[45/0/-45/90]_{3s}$, is also performed to provide reliable experimental data for FE model verification. In addition, certain defects (gaps) are intentionally placed into the specimens and their impact is experimentally evaluated. This can then be inputted into the FE model to better understand the mechanical performance of 3D printed parts as-manufactured. This research paper starts by first describing the testing methodology and defining 3D printing manufacturing process and design parameters. In a subsequent section, experimental results are presented including stress-strain graphs and Scanning Electron Microscope (SEM) images. The paper wraps up with a conclusion and recommendations for future work.

2. Methodology

This section provides information regarding ASTM D638-14 standard for determining tensile strength and modulus of FFF 3D printed specimens. Specimen design per ASTM D638-14 and the placement of intentional defects are explained. In addition, 3D printing manufacturing process and design parameters along with the 3D printer, the testing machine, and the load cell are described.

2.1. Test specimen design

The first step in the study is to design the test specimens for determining tensile strength and modulus per ASTM D638-14 [30]. There are five different specimen types, and per standard, the preferred specimen is the type I specimen for a thickness of less than 7 mm. In instances where the type I specimen does not break in the narrow section, a so called type II specimen is recommended. The type III specimen is used where the specimen thickness is between 7 and 14 mm. The type IV is usually used when non-rigid and semi-rigid materials are being compared. Finally, the type V is recommended for use in a case of limited material availability for evaluation or limited exposure space of specimens (e.g. thermal chambers).

The type I specimen is selected here since it is preferred per ASTM D638-14 and a 3D model is created in SolidWorks per geometry and dimensions given in the standard. Per ASTM D638-14, a specimen thickness of 3.2±0.4 mm is given for type I specimens where possible. In this study, specimens are designed for FFF 3D printing for a total thickness of 3.36 mm.

As explained in Section 1, manufacturing process and design parameters affect the structural performance of the 3D printed parts. The objective of this work is to characterize the mechanical properties (here tensile strength and modulus) of 3D printed parts and evaluate the impact of some specific forms of defects. As a result, among the manufacturing process and design parameter, only raster angle and the inclusion of defects were changed. A mechanical characterization approach, developed in a manner analogous to fiber-reinforced composites, is followed here. In this study, $[0]_{24}$, $[90]_{24}$, and $[45/0/-45/90]_{3S}$ stacking sequences are selected for the experimental testing. This allows researchers to use experimental data obtained along (0°) and transverse (90°) to the extrudates to build up a FE model and validate the data using quasi-isotropic layup.

3D printing machines induce defects into the final parts considering their tolerances. For the quasi-isotropic stacking sequence, $[45/0/90/-45]_{3S}$, a defect (missing extrudate/s) is placed intentionally in the 3D printed specimens to investigate its impact on their tensile strength and modulus of elasticity. Three types of defects are used here: one extrudate missing in the middle of the specimen along the length in every 0° layer; four extrudates missing in the middle of the specimen along the width in every 90° layer and; a combination of the two previous defects. Since the length of the gage section of the specimen is almost four times its width, four extrudates are not printed/extruded in a 90° layer to maintain its defect area percentage the same as the one for a missing extrudate in a 0° layer. Table 2 specifies six sets of specimens considered in this study, where the impact of defect inclusion and raster angle are investigated.

Table 2. Specimens in the test plan.

Specimen ID	Defect	Infill Raster angle (degree)
Specimen A	NO	$[0]_{24}$
Specimen B	NO	$[90]_{24}$
Specimen C	NO	$[45/0/90/-45]_{3S}$
Specimen D	1 extrudate – every 0° layer	$[45/0/90/-45]_{3S}$
Specimen E	4 extrudate – ever 90° layer	$[45/0/90/-45]_{3S}$
Specimen F	1 extrudate – every 0° layer and 4 extrudates – every 90° layer	$[45/0/90/-45]_{3S}$

2.2. Specimen manufacturing

The 3D model of the specimen is passed to Simplify3D to prepare G-codes for FFF 3D printing. Figure 1 visualizes materials deposition for specimens A, B, and C in Simplify3D software. Raster angle of 0° for specimen A, 90° for specimen B, and 45° for specimen C can be seen and there is no missing extrudate (no defect).

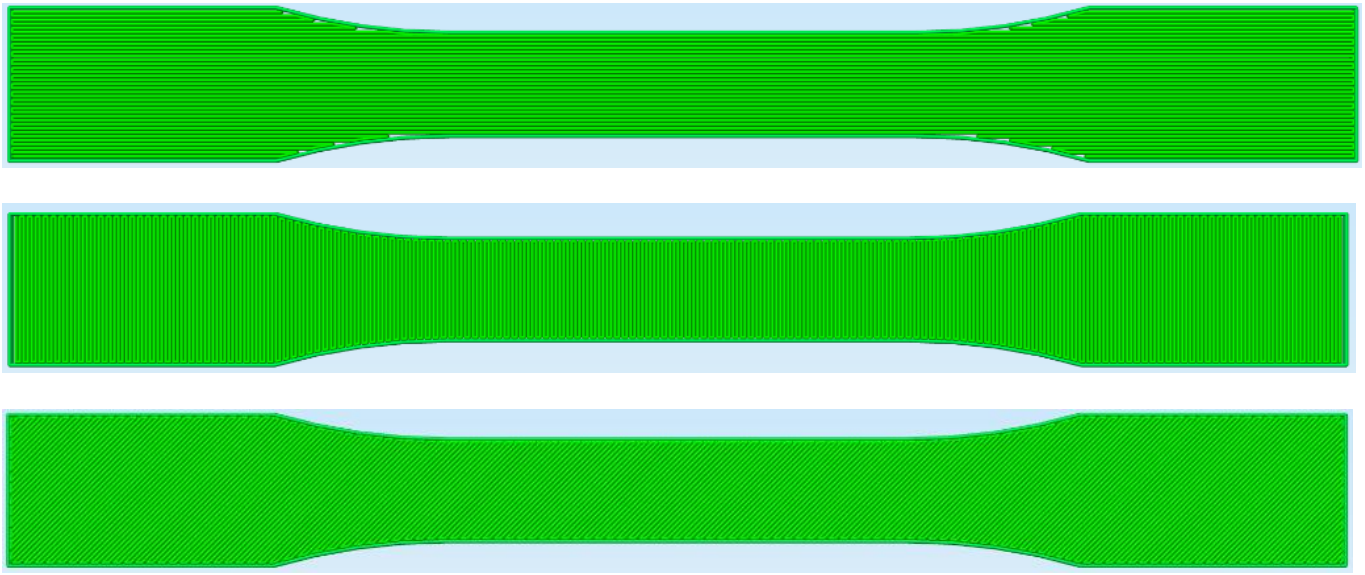

Figure 1. Materials deposition visualization in Simplify3D: (a) 0° layer-specimen A; (b) 90° layer-specimen B; (c) 45° layer for specimen C.

Figure 2 shows induced defects for specimens D, E, and F in Simplify3D software. A 0° gap (one missing extrudate) in the middle of the specimen along the length for specimen D, a 90° gap (four missing extrudates) in the middle of the specimen along the width for specimen E, and a combination of the two defects for specimen F.

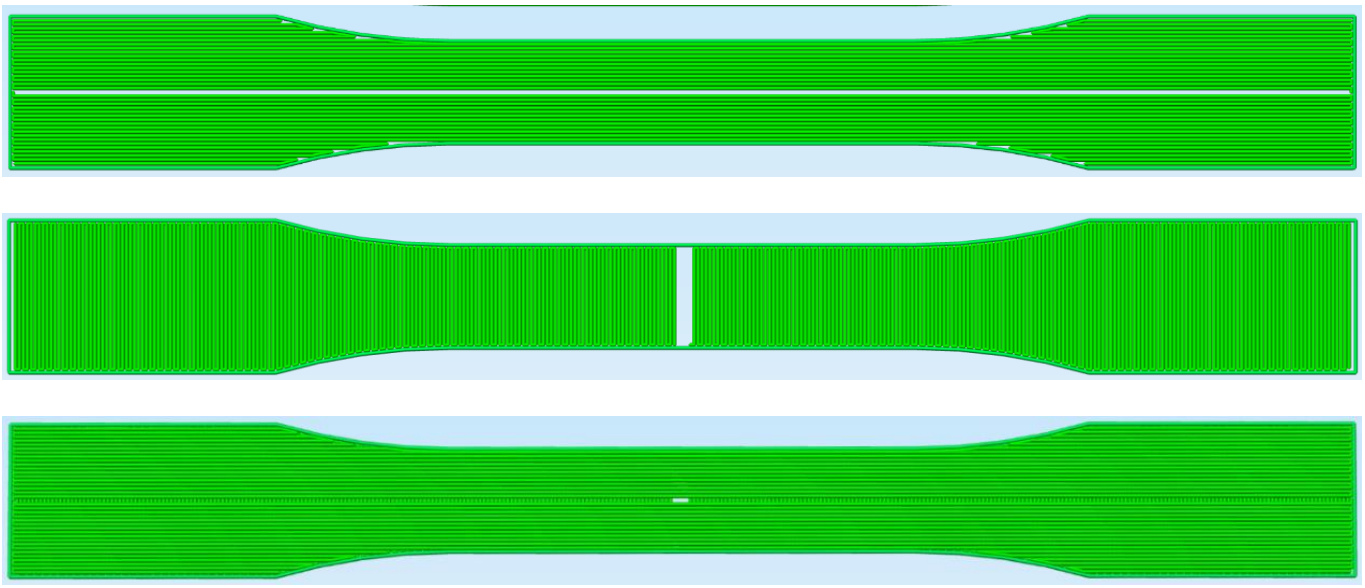

(a)

(b)

(c)

Figure 2. Defects (gaps, missing extrudates) visualization in Simplify3D: (a) 0° gap (one missing extrudate) for specimen D; (b) 90° gap (four missing extrudates) for specimen E; (c) 0° and 90° gaps for specimen F.

Five specimens per set (Table 2) were manufactured using a Prusa i3 Mk2S printer for a total of 30 specimens. Design and manufacturing process parameters are summarized in Table 3

Table 3. Manufacturing and design parameters for specimen 3D printing.

Manufacturing/design Parameter	Value	Manufacturing/design Parameter	Value
Print direction	XYZ	Material	PLA
Filament diameter	1.75 mm	Nozzle diameter	0.4 mm
Layer height	0.14 mm	Nozzle temperature	215 °C
Bed temperature	60	Cooling	No fan cooling
Printing speed	2400 mm/min	Infill %	100%
Raster angle	See Table 2	Defect inclusion	See Table 2

Figure 3 shows one 3D printed specimen per set. The material deposition orientations can be seen in the manufactured specimens without defects (Figure 3a, b, and c) that correspond to the simulated ones in Simplify3D (Figure 1a, b, and c). Furthermore, interestingly, the defect imprint in the manufactured specimens (Figure 3d, e, and f) can be seen that corresponds to the simulation in Simplify3D (Figure 2a, b, and c).

(a)

Figure 3. 3D printed PLA specimens: (a): specimen A; (b) specimen B; (c) specimen C; (d) specimen D; (e) specimen E; and (f) specimen (F).

2.3. Specimen testing and reporting

Once the manufacturing of the 30 specimens was completed, tensile testing was performed to find tensile strength, tensile modulus, and failure strain. A United mechanical testing machine with a constant displacement speed of 5 mm/min along with an extensometer is used for testing. The 30 specimens were tested to obtain failure loads and strains and further statistical analysis was performed to study the mechanical performance of the specimens. Furthermore, Scanning Electron Microscopy (SEM) imaging was utilized to analyze and compare fracture surface between specimens. SEM imaging provides crucial information regarding failure mode and gives insight into ultimate tensile strength values.

3. Results and discussion

The results are presented in two main parts: mechanical characterization of 3D printed parts without defects; and the impact of defects on tensile strength, tensile modulus, and failure strain of 3D printed parts.

3.1. Mechanical characterization of 3D printed parts without defects

Specimens A, B, and C, as described in the test plan (Table 2), are considered here. Figure 4 represents the stress–strain curve obtained for one specimen per set until failure. It should be noted that the three specimens have similar elastic moduli, which is expected for pure thermoplastic materials. However, anisotropic properties in terms of failure strength and strain due to the different raster angles during FFF 3D printing is clear in this graph.

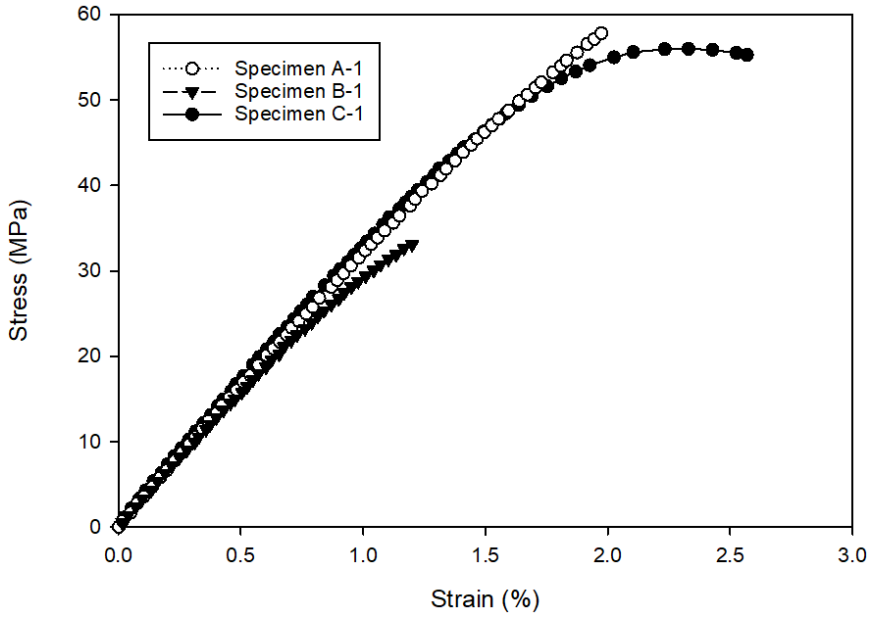

Figure 4. Stress-strain graph for specimens without defects.

The tensile modulus was calculated by a linear regression fit to the data points with R^2 of 0.999. Tensile strength, tensile modulus, and failure strain values are reported to three significant figures as per ASTM D638-14. Averages and Coefficients of Variation (CV) were calculated for each set of specimens and results are presented in Table 4.

Table 4. Tensile strength, modulus, and failure strain for specimens without defects.

Specimen ID	Mean Strength (MPa)	CV (%)	Mean modulus (MPa)	CV (%)	Mean failure strain (%)	CV (%)
Specimen A	57.7	1.1	3.13	3.0	1.96	4.4
Specimen B	30.8	12.6	2.9	3.2	1.15	12.3
Specimen C	53.5	4.2	3.11	1.8	2.35	5.5

Figure 5a, b, and c depict a the graphical representation of the testing results and include error bars based on standard deviation. By comparing the mechanical properties provided in Table 4, it can be concluded that the samples with $[0]_{24}$ stacking sequence (specimen A) have the highest tensile strength and modulus compared with $[90]_{24}$ and $[45/0/90/-45]_{3s}$ samples (specimens B and

C). This is expected for specimen A since all extrudates are along the loading direction. Specimen B with $[90]_{24}$ stacking sequence has the lowest tensile strength, modulus, and failure strain since all extrudates are transverse to the loading direction. Its tensile strength is 53% of the value for $[0]_{24}$ samples (specimen A), which confirms that FFF 3D printing induces anisotropic properties into the manufactured part. The failure strength and modulus of the quasi-isotropic $[45/0/90/-45]_{3s}$ samples (Specimen C) are close to those of $[0]_{24}$ samples (Specimen A). Yet specimen C has 20% higher failure relative to specimen A, where all extrudates are along the loading direction.

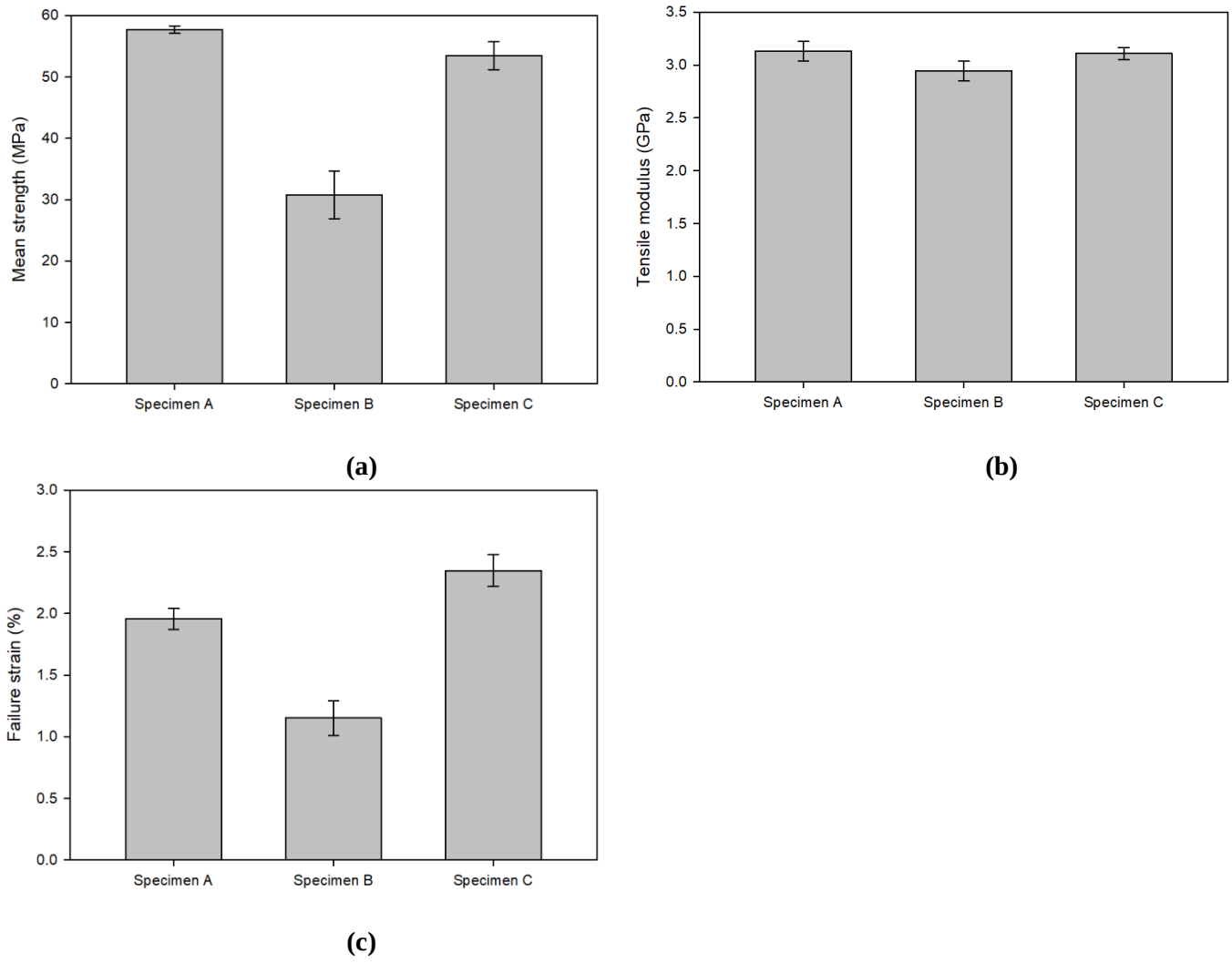

Figure 5. Mechanical performance of 3D printed specimens without defects: (a) mean tensile strength; (b) mean tensile modulus; and (c) mean failure strain.

SEM imaging for fracture surface of each sample is further provided using a magnification of 15 times (Figure 6a, b, and c). SEM imaging of specimens A-1 and C-1 fracture surface (Figure 6a and c) shows a significant deformation of extrudates cross sections and a ductile failure for the specimens, while this is not the case for specimen B-1 (Figure 6b). The similarity in the fracture

surface may further explain the close average tensile strengths and moduli for specimens A-1 and C-1.

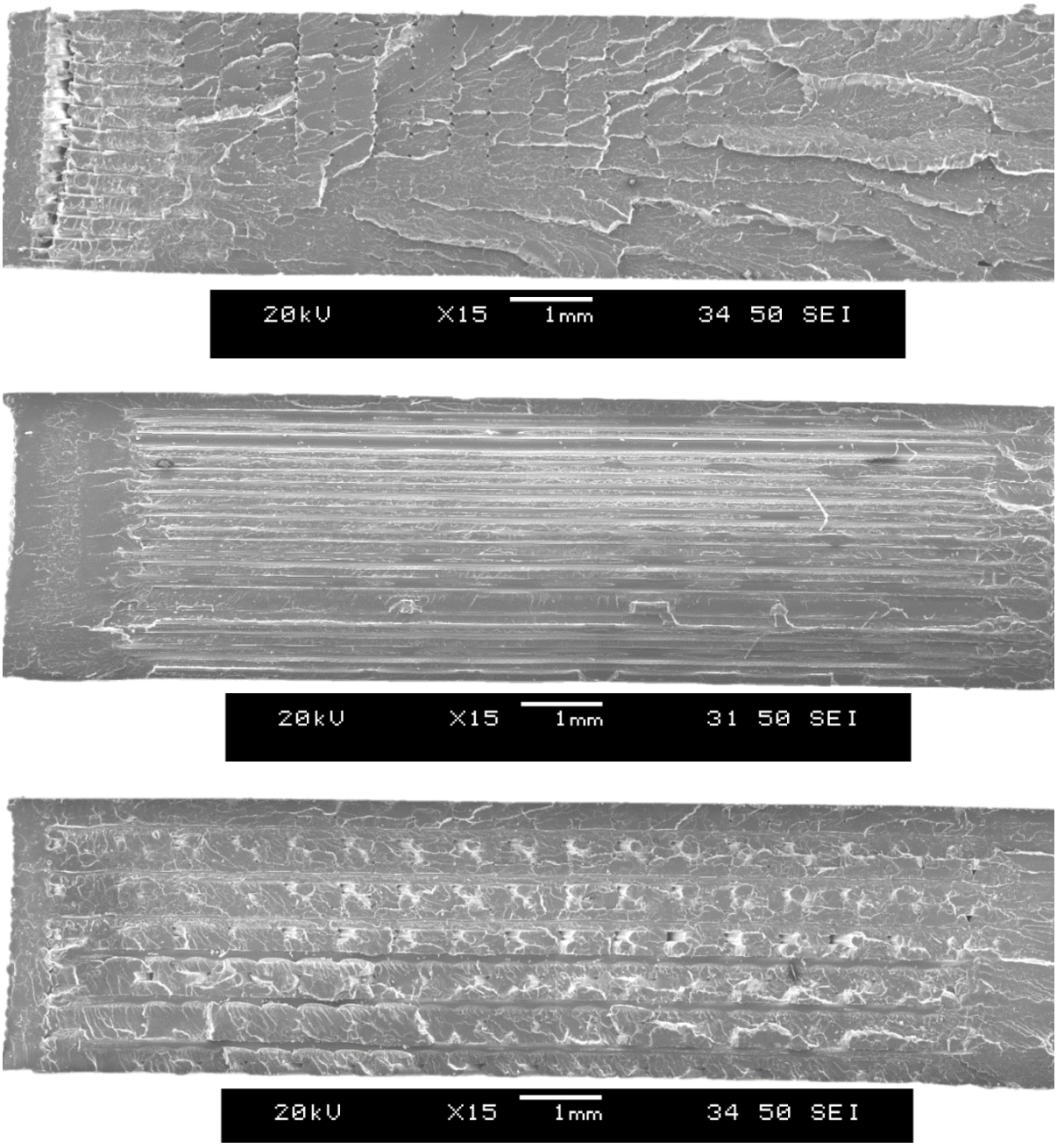

Figure 6. SEM imaging of fracture surface of specimens without defects: (a) specimen A; (b) specimen B; (c) specimen C.

3.2. Mechanical characterization of 3D printed parts with defects

Specimens D, E, and F, as described in the test plan (Table 2), are considered here. As discussed in Section 2, a quasi-isotropic layup $[45/0/90/-45]_{3s}$ (specimen C) is selected and defects

are introduced into it. Figure 7 presents the stress-strain curves obtained for one defective specimen per set along with the stress-strain curve of a non-defective one (baseline, specimen C). It can be seen that defects significantly reduce tensile strengths, while having a less pronounced impact on tensile moduli. Defective specimens (D, E, and F) have comparable tensile strengths and moduli, while specimens with 90° defect (specimens E and F) show the most reduction in failure strain, yet a highly comparable stress-strain response.

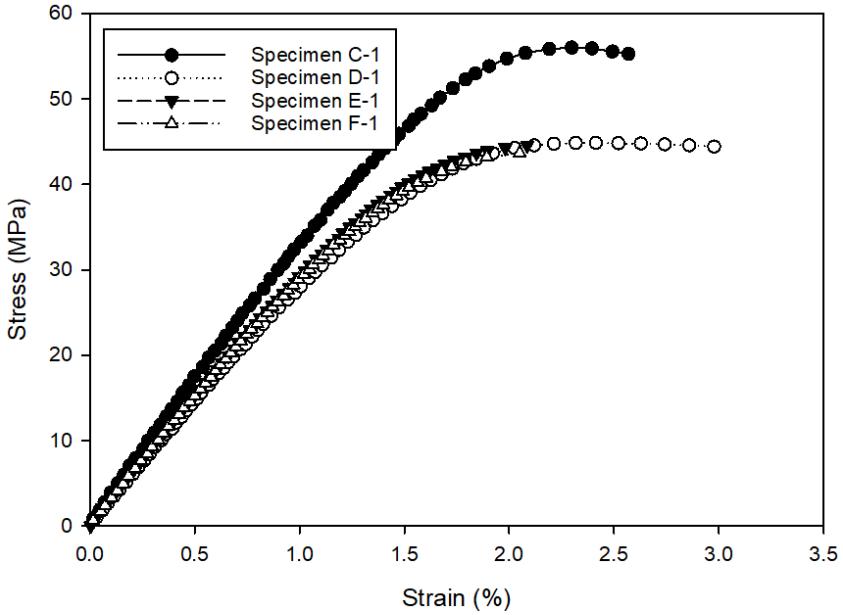

Figure 7. Stress-strain graph for the baseline and defective specimens.

The same approach, as described in Section 3.1, is followed to find the tensile moduli for the specimens. Tensile strength, tensile modulus, and failure strain values are reported to three significant figures as per ASTM D638-14. Averages and Coefficients of Variation (CV) were calculated for each set of specimens and results are presented in Table 5 along with the corresponding baseline (specimen C) data.

Table 5. Tensile strength, modulus, and failure strain for the baseline and defective specimens.

Specimen ID	Mean Strength (MPa)	CV (%)	Mean modulus (MPa)	CV (%)	Mean failure strain (%)	CV (%)
Specimen C	53.5	4.2	3.11	1.8	2.35	5.5
Specimen D	47.6	3.7	2.92	4.5	2.88	7.1
Specimen E	42.5	4.1	2.81	2.1	2.08	2.9
Specimen F	43.2	2.3	2.88	2.1	2.06	2.4

Figure 8a, b, and c present the test results, including error bars based on standard deviation. By comparing the mechanical properties provided in Table 5, it can be seen that the defect in the form of one 0° extrudate missing (specimen D) reduces tensile strength and modulus of the specimens by 12.4% and 6.1%, respectively compared with the baseline (specimen C). For the same defect area percentage as specimen D (four 90° extrudates missing, specimen E), further reduction in tensile strength (20.5%) and modulus (9.6%) is observed compared with the baseline. This can be related to the fact that the defect for specimen E is perpendicular to the loading

direction and has a more severe impact on mechanical properties compared with the defect along the loading direction in specimen D. For the combined defects case (one 0° extrudate and four 90° extrudates missing, specimen F), there is no meaningful difference in tensile strength, modulus, and failure strain with the sole four 90° extrudates missing case (specimen E). This is expected since the defect perpendicular to the loading direction (four 90° extrudates missing) causes a failure in the specimen before any significant impact from the one missing 0° extrudate.

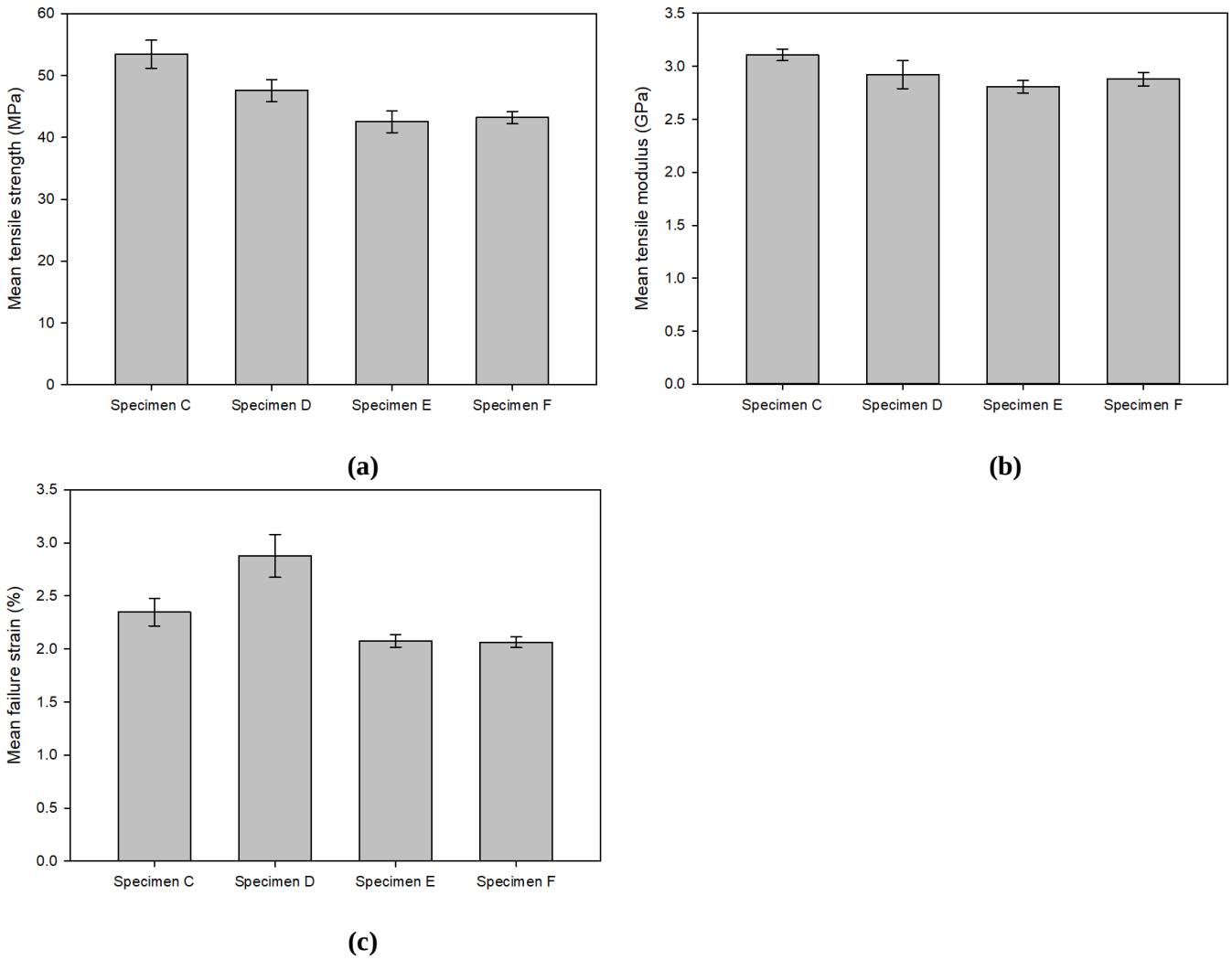

Figure 8. Mechanical performance of the baseline and defective specimens: (a) mean tensile strength; (b) mean tensile modulus; and (c) mean failure strain.

Similarly to Section 3.1, SEM imaging for fracture surface of each defective sample is provided using a magnification of 15 times (Figure 9a, b, and c). Specimen D showed 22.6% increase in failure strain compared with the baseline. For specimen D, the defect (one 0° extrudate missing) is along the loading direction and the material redistribution is the main reason behind the increase in failure strain, resulting in a ductile failure. The ductile nature of the failure for specimen D is evident from SEM imaging (Figure 9a) and it shows more deformation of extrudates cross sections compared with the baseline, specimen C (Figure 6c). Contrary to specimen D, there

was a reduction in failure strain for specimens E and F (about 11.5%) compared with the baseline. SEM images of the fracture surface for specimens E and F (Figure 9b and c) show extrudates being cut without undergoing a large strain, hence almost keeping their original cross section shape and showing brittle failure. These images show a similar pattern that further validates the closeness of the results in terms of tensile strength, modulus, and failure strain.

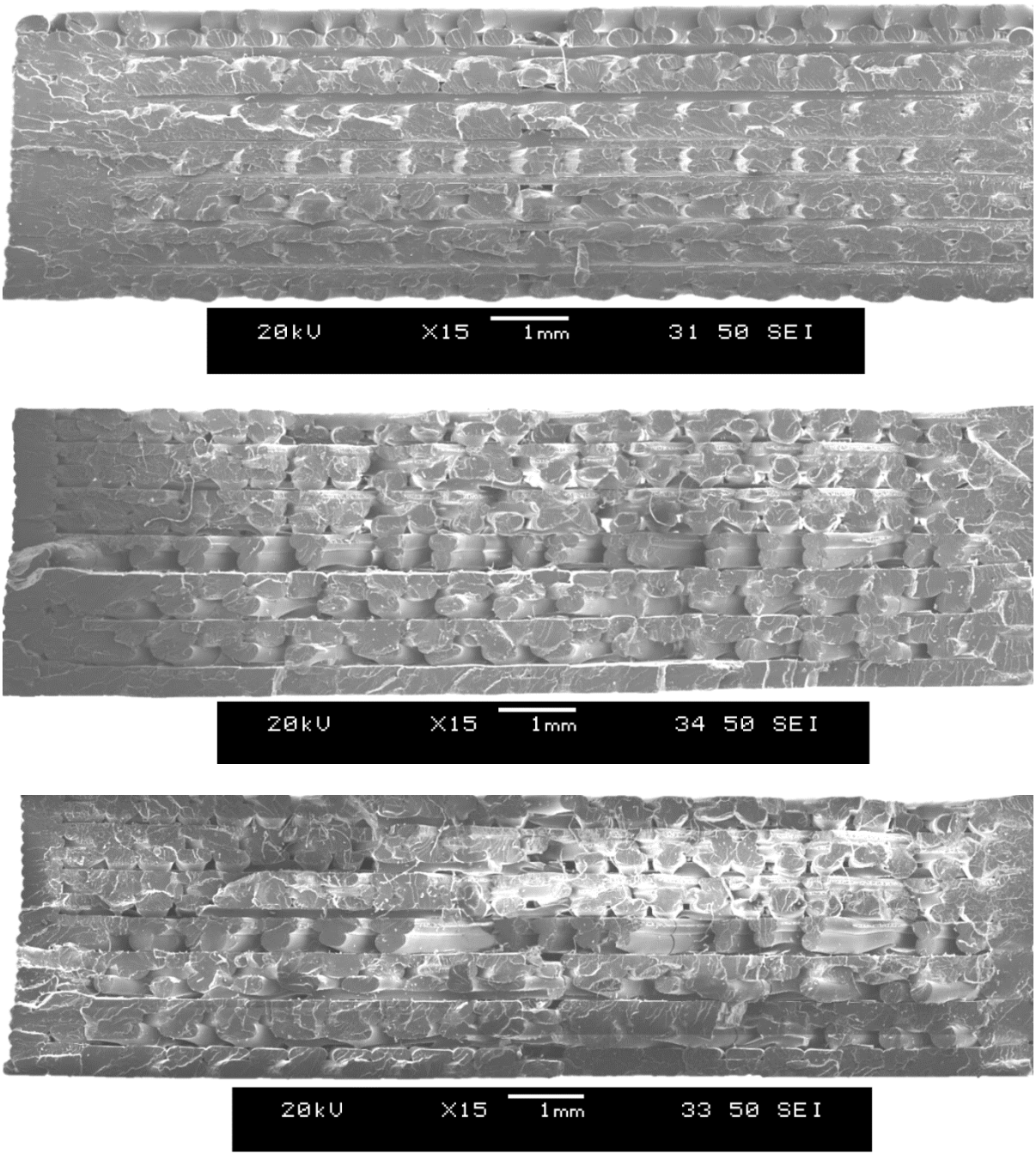

Figure 9. SEM imaging of fracture surface of specimens with defects: (a) specimen D; (b) specimen E; (c) specimen F.

4. Conclusions

In this research work, an experimental investigation of FFF 3D printed PLA parts per ASTM D638-14 has been performed. Tensile strength, modulus, and failure strain for specimens with and without defects have been obtained and SEM imaging of fracture surfaces has been captured. A systematic approach has been followed to characterize 3D printed materials, here PLA, where directional properties have been investigated

For specimens without defects, it is observed that FFF 3D printing of PLA introduces anisotropic behavior to the specimens, where printing along the loading direction ($[0]_{24}$) showed a tensile strength of 57.7 MPa compared with printing transverse to the loading direction with a tensile strength of 30.8 MPa. Quasi-isotropic stacking has 20% higher failure strain compared with the case where all extrudates are along the loading direction, $[0]_{24}$. SEM imaging of the fracture surfaces for all specimens confirms the observed trends in tensile strength, modulus, and failure strain. These results further confirm the findings by other researchers presented in Section 1. The quasi-isotropic stacking is selected as the baseline to investigate the impact of defect on mechanical performance of FFF 3D printed parts out of PLA. It is found that for the same defect area percentage, a defect transverse to the loading direction has a more severe impact on tensile strength, modulus, and failure strain compared with a defect along the loading direction. Compared with the baseline, 20.5% reduction in tensile strength, 9.6% in modulus, and 11.5% in failure strain are observed.

The approach used in this study can be followed to characterize any new material for FFF 3D printing and investigate its mechanical performance. The results presented can be further utilized in building Finite Element (FE) model of FFF 3D printed parts with and without considering the impact of defects.

Acknowledgements

The authors would like to acknowledge the financial support provided by the Natural Sciences and Engineering Research Council of Canada (NSERC). We also would like to acknowledge Dr. Hamid Ghaemi for his consultation and technical support.

Data availability

The raw/processed data required to reproduce these findings cannot be shared at this time as the data also forms part of an ongoing study.

References

1. Ravindrababu, S., et al., *Evaluation of the influence of build and print orientations of unmanned aerial vehicle parts fabricated using fused deposition modeling process.* Journal of Manufacturing Processes, 2018. **34**: p. 659-666.
2. Chacón, J.M., et al., *Additive manufacturing of PLA structures using fused deposition modelling: Effect of process parameters on mechanical properties and their optimal selection.* Materials & Design, 2017. **124**: p. 143-157.
3. Zaldivar, R.J., et al., *Influence of processing and orientation print effects on the mechanical and thermal behavior of 3D-Printed ULTEM ® 9085 Material.* Additive Manufacturing, 2017. **13**: p. 71-80.
4. Uddin, M.S., et al., *Evaluating Mechanical Properties and Failure Mechanisms of Fused Deposition Modeling Acrylonitrile Butadiene Styrene Parts.* Journal of Manufacturing Science and Engineering, 2017. **139**(8).
5. Smith, W.C. and R.W. Dean, *Structural characteristics of fused deposition modeling polycarbonate material.* Polymer Testing, 2013. **32**(8): p. 1306-1312.
6. Abouzaid, K., et al., *Printability of co-polyester using fused deposition modelling and related mechanical performance.* European Polymer Journal, 2018. **108**: p. 262-273.
7. Byberg, K.I., A.W. Gebisa, and H.G. Lemu, *Mechanical properties of ULTEM 9085 material processed by fused deposition modeling.* Polymer Testing, 2018 p. 335-347.
8. Türk, D.-A., et al., *Mechanical characterization of 3D printed polymers for fiber reinforced polymers processing.* Materials & Design, 2017. **118**: p. 256-265.
9. Fischer, M. and Schöppner V., *Fatigue Behavior of FDM Parts Manufactured with Ultem 9085.* Jom, 2016. **69**(3): p. 563-568.
10. Love, L.J., et al., *The importance of carbon fiber to polymer additive manufacturing.* Journal of Materials Research, 2014. **29**(17): p. 1893-1898.
11. Bellini, A. and Güçeri S., *Mechanical characterization of parts fabricated using fused deposition modeling.* Rapid Prototyping Journal, 2003. **9**(4): p. 252-264.
12. Safka, J., et al., *Evaluation of the Impact of Production Parameters on the Final Properties of the Part Made of Nylon 12 with Rapid Prototyping Technology (Fdm).* MM Science Journal, 2016. **2016**(03): p. 956-959.
13. Zelený, P., et al., *The Mechanical Characteristics of 3D Printed Parts According to the Build Orientation.* Applied Mechanics and Materials, 2014. **474**: p. 381-386.
14. Ziemian, S., et al., *Tensile and fatigue behavior of layered acrylonitrile butadiene styrene.* Rapid Prototyping Journal, 2015. **21**(3): p. 270-278.
15. Carneiro, O.S., et al., *Fused deposition modeling with polypropylene.* Materials & Design, 2015. **83**: p. 768-776.
16. Hill, N. and Haghi M., *Deposition direction-dependent failure criteria for fused deposition modeling polycarbonate.* Rapid Prototyping Journal, 2014. **20**(3): p. 221-227.
17. Dawoud, M., et al., *Mechanical behaviour of ABS: An experimental study using FDM and injection moulding techniques.* Journal of Manufacturing Processes, 2016. **21**: p. 39-45.
18. Gajdoš, I., et al., *Structure and tensile properties evaluation of samples produced by Fused Deposition Modeling.* Open Engineering, 2016. **6**(1): p. 86-89.
19. Mahajan, C. and Cormier D., *3D printing of carbon fiber composites with preferentially aligned fibers*. in *IIE Annual Conference. Proceedings*. 2015. Institute of Industrial and Systems Engineers (IISE): p. 2953-2962.

20. Chockalingam, K., et al., *Enhancement of anisotropic strength of fused deposited ABS parts by genetic algorithm.* Materials and Manufacturing Processes, 2016. **31**(15): p. 2001-2010.
21. Lanzotti, A., et al., *The impact of process parameters on mechanical properties of parts fabricated in PLA with an open-source 3-D printer.* Rapid Prototyping Journal, 2015. **21**(5): p. 604-617.
22. Ahn, S.-H., et al., *Anisotropic material properties of fused deposition modeling ABS.* Rapid prototyping journal, 2002. **8**(4): p. 248-257.
23. Alafaghani, A. and Qattawi, A., *Investigating the effect of fused deposition modeling processing parameters using Taguchi design of experiment method.* Journal of Manufacturing Processes, 2018. **36**: p. 164-174.
24. Ning, F., et al., *Additive manufacturing of carbon fiber-reinforced plastic composites using fused deposition modeling: Effects of process parameters on tensile properties.* Journal of Composite Materials, 2016. **51**(4): p. 451-462.
25. Garg, A. and Bhattacharya, A., *An insight to the failure of FDM parts under tensile loading: finite element analysis and experimental study.* International Journal of Mechanical Sciences, 2017. **120**: p. 225-236.
26. Vidakis, N., et al., Fused deposition modelling parts tensile strength characterisation. Academic Journal of Manufacturing Engineering, 2016. **14**(2).
27. Salem, A., et al., 3-D printing and characterization of polymer composites with different reinforcements. Advanced Processing and Manufacturing Technologies for Nanostructured and Multifunctional Materials II: Ceramic Engineering and Science Proceedings, Volume 36, 2015(6): p. 115-122.
28. ISO/ASTM 52921, *Standard Terminology for Additive Manufacturing—Coordinate Systems and Test Methodologies*. 2013. p. 1-13.
29. Popescu, D., et al., *FDM process parameters influence over the mechanical properties of polymer specimens: A review.* Polymer Testing, 2018. **69**: p. 157-166.
30. ASTM D638, *Standrd test method for tensile properties of plastics*. 2014. p. 1-17.